Neuro-Oncology 12(10):1050–1060, 2010.
doi:10.1093/neuonc/noq054
Advance Access publication July 27, 2010

Novel magnetic/ultrasound focusing system enhances nanoparticle drug delivery for glioma treatment

Pin-Yuan Chen†, Hao-Li Liu†, Mu-Yi Hua†, Hung-Wei Yang, Chiung-Yin Huang, Po-Chun Chu, Lee-Ang Lyu, I-Chou Tseng, Li-Ying Feng, Hong-Chieh Tsai, Shu-Mei Chen, Yu-Jen Lu, Jiun-Jie Wang, Tzu-Chen Yen, Yunn-Hwa Ma, Tony Wu, Jyh-Ping Chen, Jih-Ing Chuang, Jyh-Wei Shin, Chuen Hsueh, and Kuo-Chen Wei

Department of Neurosurgery, Chang-Gung University and Memorial Hospital, Taoyuan 333 (P.-Y.C., C.-Y.H., I.-C. T., L.-Y. F., H.-C.T., S.-M.C., Y.-J.L., K.-C.W.), Graduate Institute of Clinical Medical Sciences, Chang-Gung University, Taoyuan 333 (P.-Y.C., H.-C.T., S.-M.C.), Department of Electrical Engineering, Chang-Gung University, Taoyuan 333 (H.-L.L., P.-C.C., L.-A.L.), Molecular Imaging Center, Chang-Gung Memorial Hospital, Linkou 244 (H.-L.L., T.-C.Y.), Department of Chemical and Material Engineering, Chang-Gung University, Taoyuan 333 (M.-Y.H., H.-W.Y., Y.-J.L., J.-P.C.), Department of Medical Image and Radiological Sciences, Chang-Gung University, Taoyuan 333 (J.-J.W.), Department of Nuclear Medicine, Chang-Gung Memorial Hospital, Taoyuan 333 (T.-C.Y.), Department of Physiology and Pharmacology, College of Medicine, Chang-Gung University, Taoyuan 333 (Y.-H.M.), Department of Neurology, Chang-Gung University College of Medicine and Memorial Hospital, Taoyuan 333 (T.W.), Department of Physiology, National Cheng Kung University, Tainan City 701 (J.-I.C.), Department of Parasitology, National Cheng Kung University, Tainan City 701 (J.-W.S.), Department of Pathology, Chang-Gung University College of Medicine and Memorial Hospital, Taoyuan 333 (C.H.), Taiwan, Republic of China

Malignant glioma is a common and severe primary brain tumor with a high recurrence rate and an extremely high mortality rate within 2 years of diagnosis, even when surgical, radiological, and chemotherapeutic interventions are applied. Intravenously administered drugs have limited use because of their adverse systemic effects and poor blood–brain barrier penetration. Here, we combine 2 methods to increase drug delivery to brain tumors. Focused ultrasound transiently permeabilizes the blood–brain barrier, increasing passive diffusion. Subsequent application of an external magnetic field then actively enhances localization of a chemotherapeutic agent immobilized on a novel magnetic nanoparticle. Combining these techniques significantly improved the delivery of 1,3-bis(2-chloroethyl)-1-nitrosourea to rodent gliomas. Furthermore, the physicochemical properties of the nanoparticles allowed their delivery to be monitored by magnetic resonance imaging (MRI). The resulting suppression of tumor progression without damaging the normal regions of the brain was verified by MRI and histological examination. This noninvasive, reversible technique promises to provide a more effective and tolerable means of tumor treatment, with lower therapeutic doses and concurrent clinical monitoring.

Keywords: BCNU, glioma, magnetic nanoparticle, MRI, ultrasound.

Received June 25, 2009; accepted March 29, 2010.

†These authors contributed equally to this work.

Corresponding Author: Dr. Kuo-Chen Wei, MD, Department of Neurosurgery, Chang-Gung University College of Medicine and Memorial Hospital, 5 Fu-Shing St., Kwei-Shan Taoyuan 333, Taiwan, Republic of China (kuochenwei@cgmh.org.tw).

Malignant glioma is a devastating disease with an extremely high mortality rate within 2 years of diagnosis, even when surgical, radiological, and chemotherapeutic interventions are applied.[1,2] Gliomas are commonly treated by gross

total excision, and complete tumor resection correlates with a better clinical outcome and improved neurological function.[3] However, because such tumors are often infiltrative, total resection of all tumor cells is difficult to achieve,[4] resulting in poor prognosis. Subsequent treatments with intravenously administered chemotherapeutic drugs have limited use because of their adverse systemic effects and poor blood–brain barrier penetration.[5–9]

A number of different strategies have been explored for more effective drug delivery.[10–14] Targeting of nanoparticles by an externally applied magnetic field is one safe and promising strategy for achieving localized drug delivery, even in deep-seated brain tumors.[15–18] Likewise, recent studies have shown that high-intensity focused ultrasound can be used to transiently disrupt the blood–brain barrier without damaging the surrounding neural tissue.[19–23] Furthermore, the effects of this technique can be monitored by magnetic resonance imaging (MRI).[19,24] In the present study, we used focused ultrasound to permeabilize the blood–brain barrier transiently, followed by the application of an external magnetic field. Combined use of these innovative techniques significantly improved the delivery of 1,3-bis(2-chloroethyl)-1-nitrosourea (BCNU) immobilized on a novel magnetic nanoparticle (MNP) to gliomas in a rodent model. Dramatic tumor shrinkage was verified by a serial MRI and histological examinations. Furthermore, treatment with the magnetic/ultrasound system prolonged the survival of the rats. This novel strategy offers an effective way to deliver anticancer drugs or molecules to brain tumors, with the potential for concurrent clinical monitoring.

Materials and Methods

Preparation of MNPs

Details of this procedure appear in the Supplementary Data. Briefly, poly[aniline-*co*-sodium *N*-(1-one-butyric acid)] aniline (SPAnNa) was prepared using supercritical carbon dioxide as the reaction medium and subsequently transformed into poly[aniline-*co*-*N*-(1-one-butyric acid)] aniline (SPAnH) using a H^+-type cation exchange resin; SPAnH contains –COOH functional groups capable of immobilizing BCNU. A solution of Fe_3O_4 was mixed with the SPAnNa solution and the mixture was doped slowly by addition of 0.5 M HCl. Acid doping of SPAnNa induces formation and aggregation of SPAnH. Fe_3O_4 nanoparticles are encapsulated during the aggregation, forming the Fe_3O_4/SPAnH nanoparticles. These magnetic composites were separated from the solution using a strong magnet and washed with deionized water until the pH was neutralized. Fe_3O_4/SPAnH nanoparticles were dispersed in deionized water and analyzed by Fourier transform infrared (FT-IR) spectroscopy. The saturated magnetization strength of the particles was determined using a superconducting quantum interference device (SQUID).

Immobilization of BCNU on MNPs

Twelve milligrams of 1-ethyl-3-(3-dimethylaminopropyl) carbodiimide and 24 mg of *N*-hydroxysulfosuccinimide were dissolved in 2 mL of 0.5 M 2-morpholinoethanesulfonic acid (MES; pH 6.3) in the dark. A 0.1-mL aliquot of the solution was mixed with 0.2 mL of the Fe_3O_4/SPAnH nanoparticles (10 mg/mL) and sonicated for 1 hour at 25°C. The nanoparticles were separated magnetically from the solution, washed once with 0.8 mL of 0.1 M MES, then magnetically separated again and suspended in 0.2 mL of MES. A 0.2-mL aliquot of the nanoparticle solution was mixed with 0.1 mL of BCNU (5 mg/mL) and sonicated for 2 hours at 15°C. After sonication, the BCNU–MNPs were separated from the solution and mixed with 0.7 mL pure alcohol. The composite-free solute was analyzed by high-performance liquid chromatography (HPLC) using an L-2130 pump and an L-2400 UV-detector (Hitachi) on a SUPELCOSIL™ LC-18 column (4.6 × 250 mm) using a mobile phase of deionized water:methanol (40:60) at a flow rate of 2 mL/min and a measuring wavelength of 270 nm. The alcohol was washed from the MNPs with deionized water and the MNPs were dispersed in 0.2 mL deionized water.

Activity Assay of Immobilized BCNU

The activity of BCNU immobilized on the MNPs was analyzed using the Bratton–Marshall method.[25,26] Briefly, 40 μL of the BCNU–MNP solution were mixed with 80 μL of sulfanilamide (5 mg/mL in 2 M HCl) and incubated for 45 minutes at 50°C. The samples were cooled to room temperature and 100 μL of the reaction product were treated with 10 μL of *N*-(1-naphthyl) ethylenediamine (3 mg/mL in deionized water) for 1 minute. The relative activity was determined by measuring the absorption peak by UV-Vis–near-IR spectroscopy at 540 nm.

In Vitro Cytotoxicity Assay

Rat glioma C6 cells were cultured in RPMI 1640 medium containing 2.2 mg/mL of hydrogen sodium carbonate, 10% fetal bovine serum, 50 μg/mL of gentamycin, 50 μg/mL of penicillin, and 50 μg/mL of streptomycin at 37°C in an atmosphere of 5% CO_2. Cells were harvested by trypsinization for 2 minutes (0.2 mg/mL of trypsin, 0.08 mg/mL of EDTA), scraped from the culture dishes, and transferred to centrifuge tubes. Cells were pelleted by centrifugation at 1500 rpm for 8 minutes at 8°C. The supernatant was removed and the C6 cells were resuspended in fresh culture medium to a concentration of $\sim 6.67 \times 10^4$ cells/mL. Aliquots containing ~10 000 cells (ie, 150 μL) were placed in each well of a 96-well culture plate and incubated in a humidified chamber at 37°C and 5% CO_2 for 24 hours. Fifty microliters of BCNU (20 or 100 μM) or BCNU–MNPs (20 or 100 μM) in culture medium were added to each well and the plates returned to the incubator.

Cytotoxicity was assessed at 2, 4, 8, 12, 24, 48, and 72 hours after the addition of the drugs. The culture medium was removed from each well and replaced with 120 μL of sodium 3′-[1-(phenylaminocarbonyl)-3,4-tetrazolium]-bis (4-methoxy-6-nitro) benzene sulfonic acid hydrate (XTT) reagent, and the samples incubated for 3 hours at 37°C. One-hundred-microliter aliquots of the reacted XTT solution were transferred from each culture well to a fresh 96-well ELISA plate, and the cytotoxicity was evaluated by measuring the optical density of the XTT solution at 490 nm.

Animals

Pathogen-free male Sprague–Dawley rats weighing ~300 g (14–18 weeks old) were purchased from BioLASCO. All animal experiments were conducted according to the protocols approved by Chang-Gung University's Institutional Animal Care and Use Committee.

Focused Ultrasound Treatment

A focused ultrasound transducer (Imasonics; diameter = 60 mm, radius of curvature = 80 mm, frequency = 400 kHz, electric-to-acoustic efficiency = 70%) was used to generate concentrated ultrasound energy. An arbitrary-function generator (33 120A, Agilent; and DS345, Stanford Research Systems) was used to produce the driving signal, which was fed to a radio frequency power amplifier (150A100B, Amplifier Research) operating in burst mode. The focal zone distribution of the intensity of the ultrasound field was measured in an acrylic water tank filled with deionized, degassed water, with the transducer attached to a semiautomatic 3D positioning system. A PVDF-type hydrophone (Onda; calibration range: 50 kHz to 20 MHz) was used to measure the pressure distribution radially and along the transducer axis. The measured diameter of the half-maximum pressure amplitude was ~3 mm, and the length of the produced focal zone was ~15 mm.

Before ultrasound treatment, animals were anesthetized by i.p. injection of chlorohydrate (30 mg/kg). The top of the cranium was shaved with clippers, and a PE-50 catheter was inserted into the jugular vein for injections. The animal was placed directly under an acrylic water tank (with a window of 4 × 4 cm^2 at its bottom sealed with a thin film to allow entry of the ultrasound energy) with its head attached tightly to the thin-film window. SonoVue® SF_6-coated ultrasound microbubbles (2–5-μm mean diameter, 2.5 μg/kg; Bracco Diagnostics Inc.) were administered intravenously before treatment. Moderate ultrasound power (2 W, equivalent to a peak negative pressure of 0.7 MPa) was delivered to the brain with the center of the focal zone positioned at a penetration depth of 2–3 mm in each hemisphere. Burst-mode ultrasound was used, with a burst length of 10 ms, a pulse-repetition frequency of 1 Hz, and a total sonication duration of ~30 s.

Magnetic Field Targeting

After focused ultrasound treatment, a neodymium–iron–boron permanent magnet with a maximum magnetic flux density of 3000 Gauss was used to produce an inhomogeneous magnetic field. The magnet was fixed securely to the cranium of rats receiving the magnetic targeting treatment. The magnetic field was applied for up to 24 h after MNP injection.

Magnetic Resonance Imaging

All MRI images were acquired on a 3 T scanner (Trio with Tim; Siemens) using the standard wrist coil with an inner diameter of 13 cm. The animals were anesthetized with a 1.5%-isoflurane/air mixture, placed in an acrylic holder and positioned in the center of the magnet. An i.v. bolus (0.1 mmol/kg) of gadopentetate dimeglumine MRI contrast agent (Magnevist; Berlex Laboratories) was administered before scanning. To quantify the tumor size and to identify the region of blood–brain barrier disruption induced by focused ultrasound, contrast-enhanced T1-turbo-spin-echo sequences were acquired using the following parameters: TR/TE = 421 ms/11 ms, slice thickness = 0.7 mm, matrix size = 128 × 256, FOV = 39 × 60 mm (resolution = 0.3 × 0.3 mm). Tumor size was also quantified using T2-weighted images with the following parameters: TR/TE = 2510 ms/94 ms, matrix size = 128 × 256, FOV = 39 × 60 mm (resolution = 0.3 × 0.3 mm). Heavy T2*-weighted 3D fast low-angle shot sequences with full-flow compensation in all 3 directions have high sensitivity for image susceptibility changes caused by superparamagnetic iron oxide particles and were used to detect image changes caused by local deposition of BCNU–MNPs.[27] Images were acquired using the following parameters: TR/TE/flip angle = 28 ms/20 ms/15°, matrix size = 128 × 384, FOV = 43 × 130 mm (resolution = 0.3 × 0.3 mm), slice thickness = 0.7 mm, which gave a voxel size of 0.3 × 0.3 × 0.7 mm^3.

Quantitative Analysis of MNP Distribution in Normal Rat Brain

Normal healthy rats were divided into 5 treatment groups ($n = 3$). Control rats received no treatment. The second group received a single dose of BCNU–MNPs administered via the external jugular vein. The third group was subjected to focused ultrasound treatment before MNP administration. The fourth group was injected with MNPs and subsequently subjected to an externally applied magnetic field. The fifth group was subjected to a combined treatment of ultrasound before, and magnetic targeting after, particle injection. Rats were sacrificed 24 hours after treatment. Brains were collected immediately, washed twice with normal saline, and dried under vacuum for 48 hours at 80°C. The dried samples were ground into powder, and the powders were acid-digested in 13 M aqua regia using a DC300H sonicator (Taiwan Delta New Instrument Co.) at 60°C for 1 hour. The

iron content of the samples was measured using a 700-ES inductively coupled plasma optical emission spectroscopy (ICP–OES) system (Varian Inc.). Each assay was performed in triplicate.

C6 Rat Brain Tumor Model

C6 rat glioma cells were cultured at 37°C in a humidified 5% CO_2 atmosphere in Minimum Essential Medium supplemented with 10% fetal bovine serum and 1% penicillin/streptomycin (Invitrogen). Cells were harvested by trypsinization, washed once with phosphate-buffered saline, and resuspended (1×10^5 cells/μL) in Minimum Essential Medium for implantation into the striatum of rat brains. Male Sprague–Dawley rats (320–350 g) were anesthetized by i.p. administration of ketamine (100 mg/kg) and immobilized on a stereotactic frame. A sagittal incision was made through the skin overlying the calvarium, and a small dental drill was used to make a hole in the exposed cranium 0.5 mm anterior and 3 mm lateral to the bregma. Five microliters of the C6 cell suspension were injected at a depth of 4.5 mm from the brain surface. The injection was performed over a 10-min period, and the needle was withdrawn over another 2 min.

In Vivo Treatment Groups

Several groups of rats with tumors induced as described above were subjected to different treatment protocols (Table 1). Except where indicated, each group consisted of at least 5 subjects. Control rats (Group 1; $n = 14$) were injected with C6 glioma cells but received no further treatment. All therapeutic treatments consisted of a single dose administered via the external jugular vein after the tumors became apparent (usually 17 days after glioma cell injection). Group 2 rats received a single dose of free (ie, nonparticle-bound) BCNU (13.5 mg/kg). Group 3 rats were subjected to a sham procedure, in which 0.5 mL of normal saline (without particles) was injected i.v., followed by focused ultrasound/magnetic targeting. Animals in Group 4 ($n = 3$) were injected with 0.5 mL of an 8-mg/kg solution of drug-free MNPs (ie, without bound BCNU).

Three groups of animals (Groups 5, 7, and 9) received varying doses of particle-bound BCNU but no magnetic/ultrasound treatment; another 3 groups (6, 8, and 10) received the same range of doses, but were subjected to the magnetic/ultrasound focusing system. Groups 5 and 6 (high dose) received 0.5 mL of 8-mg/mL BCNU–MNPs. Assuming a drug concentration of 420 μg of BCNU per mg of MNPs (Fig. 1F), a rat weighing 330 g would receive a dose of 1.68 mg BCNU ($0.5 \times 8 \times 0.42$), or 5.09 mg BCNU/kg body weight. Rats in Groups 7 and 8 received an intermediate dose corresponding to 1 mg BCNU/kg body weight, and Groups 9 and 10 (low dose) received only 0.5 mg BCNU/kg body weight.

Animals were assessed by MRI before and immediately after magnetic/ultrasound treatment (to detect focused ultrasound-induced blood–brain barrier disruption and particle distribution) and at 1-week intervals after treatment (to determine tumor size). The changes in average tumor volume were determined 1 week after treatment and their ratios to initial tumor volumes were compared using one-way ANOVA and post hoc tests. Selected groups were monitored for longer periods to determine their survival rates, which were analyzed by log-rank tests and Kaplan–Meier estimations. Two additional rats for each group were prepared and sacrificed for histological or electron microscopic examinations; these animals were not included in tumor volume or survival analyses.

Histology

Histopathological examinations were performed on normal rats to quantify MNP accumulation, and on tumor-bearing rats subjected to various treatment protocols. Excised tissue samples were fixed immediately in 10% neutral-buffered formalin for 24 hours at room temperature. The samples were dehydrated in ethanol, embedded in paraffin, sectioned, and stained with hematoxylin and eosin or Prussian blue (a stain specific for the identification of iron). Immunohistochemical studies were performed using primary antibodies against the S100 protein (diluted 1:500; Dako) or CD68 (diluted 1:200; Dako) for identification of tumor cells and

Table 1. Experimental conditions for in vivo treatment groups

Group no.	Group name	i.v. Administration	Treatment	No. of animals
1	Control	—	—	14
2	BCNU-only	Unbound BCNU (13 mg/kg)	—	6
3	M/U (sham)	—	Mag/FUS	6
4	MNP-only	8 mg/kg MNPs (w/o BCNU)	—	3
5	High-dose control	BCNU–MNPs (5 mg/kg)	—	6
6	High-dose exp.	BCNU–MNPs (5 mg/kg)	Mag/FUS	6
7	Medium dose control	BCNU–MNPs (1 mg/kg)	—	6
8	Medium dose exp.	BCNU–MNPs (1 mg/kg)	Mag/FUS	6
9	Low dose control	BCNU–MNPs (0.5 mg/kg)	—	5
10	Low dose exp.	BCNU–MNPs (0.5 mg/kg)	Mag/FUS	6

Mag/FUS, magnetic/ultrasound focusing system enhancement.

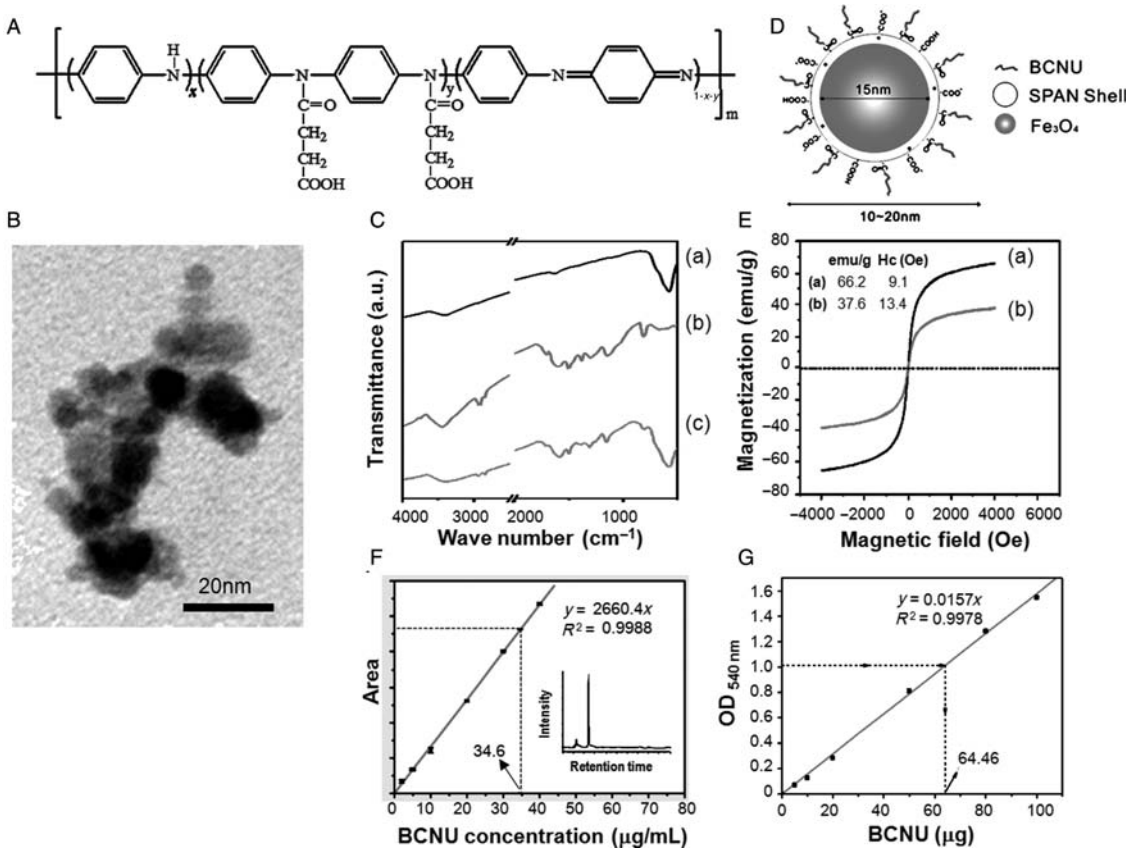

Fig. 1. (A) Structure of poly[aniline-*co*-*N*-(1-one-butyric acid)] aniline (SPAnH). (B) Transmission electronic micrograph of SPAnH nanoparticles. (C) FT-IR spectra at room temperature of (A) Fe_3O_4, (B) SPAnH, and (C) Fe_3O_4/SPAnH nanoparticles. (D) Schematic representation of BCNU immobilized on a polyaniline shell surrounding a magnetic nanoparticle core. (E) SQUID spectra at room temperature showing the superparamagnetic properties of (A) Fe_3O_4 and (B) the Fe_3O_4/SPAnH nanoparticle. (F) Standard curve and HPLC spectrum (inset) of BCNU. (G) Standard curve of BCNU activity as assessed by the Bratton–Marshall assay. The functional efficacy of 80.3 mg bound BCNU is equal to that of 64.46 mg unbound BCNU.

macrophages/microglia, respectively. Sections were washed and incubated with rabbit anti-mouse IgG (1:100; Dako). Avidin–biotin complexes (Dako) and the chromogen 3-amino-9-ethylcarbazole (Dako) were used for visualization. Sections were counterstained lightly with hematoxylin. All histological samples were examined by a single experienced neuropathologist blinded to the treatment protocols.

Transmission Electron Microscopy

Fresh cells or tissues were fixed in phosphate buffer containing 30 mg/mL glutaraldehyde, postfixed in 10 mg/mL osmium tetroxide, dehydrated through a graded series of alcohol, and finally embedded in Epon 812. Ultrathin sections (50 nm) were stained with uranyl acetate and lead citrate and examined using a Hitachi H-7500 transmission electron microscope.

Results

For this study, a novel MNP of Fe_3O_4 coated with SPAnH (Fig. 1A) was developed. This water-soluble material has carboxylic acid side chains that can bind drugs easily. The size of the particles was ~10–20 nm, as determined by transmission electron microscopy (Fig. 1B). Characterization of the Fe_3O_4/SPAnH nanoparticle structure by FT-IR spectroscopy (Fig. 1C; also see Supplementary Data) indicated that the surface of the Fe_3O_4 particle was covered with a layer of the SPAnH polymer, and that the outermost layer of the composite maintained the –NH and –COOH groups, which could be used for the immobilization of biomaterials or drugs (Fig. 1D). Furthermore, when the saturated magnetization strength of the particles was measured using a SQUID, the residue magnetization and coercivity were zero and no magnetic hysteresis loop was observed, indicating typical superparamagnetic behavior for the MNPs (Fig. 1E). The saturated magnetization of Fe_3O_4 and Fe_3O_4/SPAnH composites were 66.2 and 37.6 emu/g, respectively; the apparent reduction is because the Fe_3O_4 represents only a portion of the gram weight of the composite, resulting in a decrease in the per-unit saturated magnetization strength.

BCNU was then bound covalently to the MNPs. The immobilization ratio was 86.2% as analyzed by HPLC (Fig. 1F), which corresponds to 420 μg of BCNU fixed

per mg of MNP. The Bratton–Marshall assay revealed a functional efficacy of particle-bound BCNU that was ~80% that of unbound BCNU (Fig. 1G).

MNPs with immobilized BCNU (100 μM) easily entered C6 tumor cells by active phagocytosis within 24 hours (Fig. 2B). The cytotoxicities of the Fe_3O_4/SPAnH nanoparticles, unbound BCNU, and BCNU–MNPs on these cells were determined using an XTT assay (Fig. 2A). The Fe_3O_4/SPAnH nanoparticles displayed no cytotoxicity in rat glioma C6 cells up to 72 hours, whereas a dose of 20 μM BCNU–MNPs inhibited cell growth by ~30% at 8 hours. The cytotoxicity of BCNU–MNPs was dose-dependent; at 100 μM, cell growth was inhibited up to 52% at 8 hours, and the effect was sustained for at least 72 hours. At 72 hours, the toxicities of bound BCNU were 78% (100 mM) and 82% (20 mM) those of unbound BCNU. These results were consistent with those of the Bratton–Marshall assay and revealed that immobilization of BCNU on the nanoparticle composites did not significantly alter its toxicity.

Normal healthy rats were subjected to various treatments to determine their efficacy in delivering localized concentrations of MNPs to a specific region of the brain. Quantitative analysis of iron content by ICP–OES revealed that when focused ultrasound or magnetic targeting was applied alone, it only increased particle concentration in the treated portion of the brain by 2-fold relative to the untreated region. Dramatically, however, when the combined magnetic/ultrasound focusing system was used, particle accumulation in the treated area increased 9.9-fold relative to the untreated region, and nearly 26-fold relative to animals injected with MNPs but receiving no additional treatment (Fig. 3A). After 24 hours of treatment, heavy T2* susceptibility-weighted imaging showed a greater accumulation of MNPs in the brains of animals subjected to the magnetic/ultrasound focusing system than when either method was used separately (Fig. 3B). Histological examination of the brains of rats sacrificed after 24 hours of treatment confirmed the accumulation of the MNPs in the brain (Fig. 3C).

MRIs of tumor-implanted animals were performed before and after the animals underwent treatment with the magnetic/ultrasound focusing system to deliver the BCNU–MNPs (Fig. 4). Gadolinium-based contrast-enhanced T1-weighted images showed that disruption of the blood–brain barrier could be focused on the peritumoral region. Additionally, T2-weighted imaging showed that treatment with the magnetic/ultrasound focusing system did not induce additional lesions (eg, hemorrhaging). Furthermore, heavy T2*-weighted images were able to display the distribution of the superparamagnetic iron oxide particles, demonstrating the efficacy of the targeting effect.

Tumor-implanted animals were examined 1 week after treatment and tumor shrinkage was assessed by calculating the ratio of the tumor volume after treatment to the pretreatment volume (Fig. 5A and B). Animals in the control (ie, no treatment), BCNU-only, nanoparticle-only, and sham procedure (magnetic/ultrasound focusing-only) groups showed no tumor shrinkage during the first week. However, tumor volumes were suppressed in the first week in groups receiving a high dose of BCNU (5 mg/kg), regardless of whether focused ultrasound and magnetic targeting were applied (Group 6: tumor volume ratio = -0.97 ± 0.08) or not (Group 5: -0.52 ± 0.69). The medium dose (1 mg/kg) appeared to represent a critical threshold: Tumor growth was suppressed when magnetic/

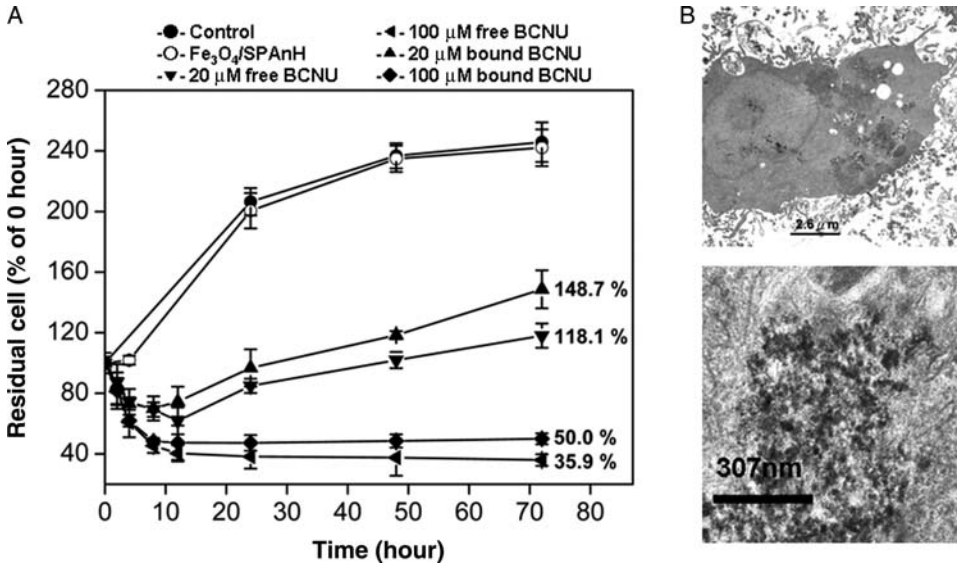

Fig. 2. (A) Cytotoxicity of free and nanoparticle-immobilized BCNU in rat glioma C6 cells. Control (●); Fe_3O_4/SPAnH nanoparticles (○); BCNU–MNPs, (20μM; ▲) and (100 μM; ◆); free BCNU (20 μM;▼) and (100 μM; ◄). (B) Transmission electron micrographs of C6 cells indicating phagocytosis of MNPs.

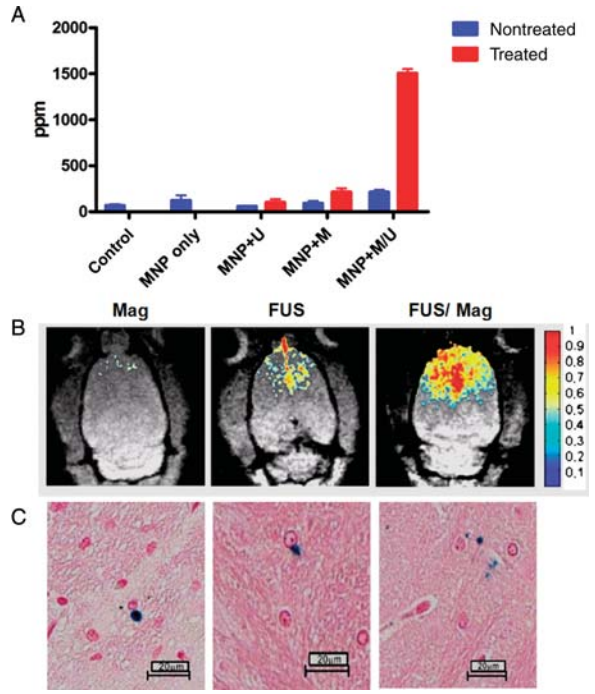

Fig. 3. (A) Distribution of BCNU-MNPs in normal rat brain as assessed by ICP–OES after different treatments. Treated and untreated regions of the brain are also compared. Focused ultrasound (U) or magnetic guidance (M) alone each only slightly improved particle accumulation in the brain. The magnetic/ultrasound focusing system (M/U) dramatically increased MNP concentration at the treatment site. (B) Heavy T2*-weighted images and (C) histological sections confirm the accumulation of MNPs using the M/U system (right) compared with M (left) or U (center) alone.

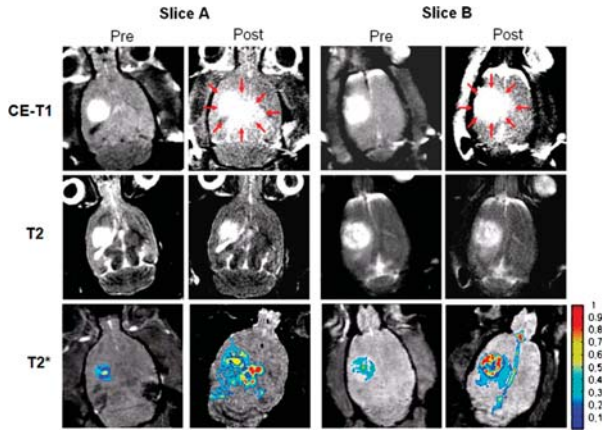

Fig. 4. Representative MRIs of tumor-implanted animals before and after undergoing magnetic/ultrasound focusing enhancement of BCNU-MNP delivery. Images from 2 adjacent slices are shown. Upper: gadolinium-based contrast-enhanced T1-weighted images (the blood–brain barrier-disrupted areas are indicated by red arrows); middle: T2-weighted images; lower: Heavy T2*-weighted images.

ultrasound focusing was applied (Group 8: -0.79 ± 0.35), but progressed in the sham group (Group 7: 2.96 ± 3.0). The lowest dose of BCNU–MNPs tested was unable to suppress tumor progression either without (Group 9: 1.63 ± 1.94) or with (Group 10: 0.31 ± 0.84) magnetic/ultrasound focusing treatment, although the combined application of magnetic targeting and focused ultrasound did appear to slow progression somewhat. Post hoc analysis confirmed that the tumor volume ratios of Groups 5, 6, 8, and 10 were significantly different from that of Group 1 ($P < 0.05$; see Supplementary Data, Table 2).

Histological examination of tissues from treated brains showed that infiltration of CD68-positive cells into tumors did not increase during the first 3 days post-treatment (relative to tumors from the control group), but did increase after tumor necrosis and shrinkage (Fig. 6A). Furthermore, the CD68-positive cells remained in situ after tumor shrinkage. Prussian blue staining showed that the iron deposits (from the MNPs) occurred primarily in the CD68-positive cells. However, transmission electron microscopic examination of tumor specimens showed that the particles were also taken up tumor cells and cells undergoing apoptosis as early as 1 day posttreatment.

Discussion

Effective delivery of chemotherapeutic agents past the blood–brain barrier remains a major challenge in the postoperative treatment of gliomas.[5–7,13,14] Numerous innovative techniques have been used to overcome this obstacle. Vascular permeability can be enhanced by intra-arterial administration of hyperosmotic solutions[11] or by treatment with CD8 T cells[9] or vascular endothelial growth factor.[10] Alternatively, drugs can be delivered to the tumor by conjugation or chimerization to peptides known to undergo receptor-mediated transcytosis across the barrier.[8,12]

The vascular and hemodynamic characteristics of brain tumors are distinctly different from those of intact brain tissue, and include features such as reduced vascular density, increased capillary diameter, and markedly decreased blood flow.[28–30] Because the efficiency of magnetic capture of MNPs is inversely related to the flow rate of the carrier medium, brain tumors are particularly suitable for magnetic targeting. Previous reports showed that the concentration of MNPs in tumors can be enhanced by magnetic targeting.[17,31] Nevertheless, the failure to achieve uniform therapeutic drug concentrations in brain tumors can still be attributed to the impermeable nature of the blood–brain barrier.[32] Indeed, disruption of the blood–brain barrier by tumors is highly heterogeneous,[33–36] and permeability can vary widely within different areas of the same tumor. Also, permeability does not necessarily correlate with tumor histology, size, or anatomical location. Consequently, not all cells within a tumor will necessarily receive the same dose of a therapeutic agent. Because magnetic guidance can limit retention of MNPs to a specific part of a tumor, the use of focused ultrasound to open the blood–brain barrier in that same region can synergize with the

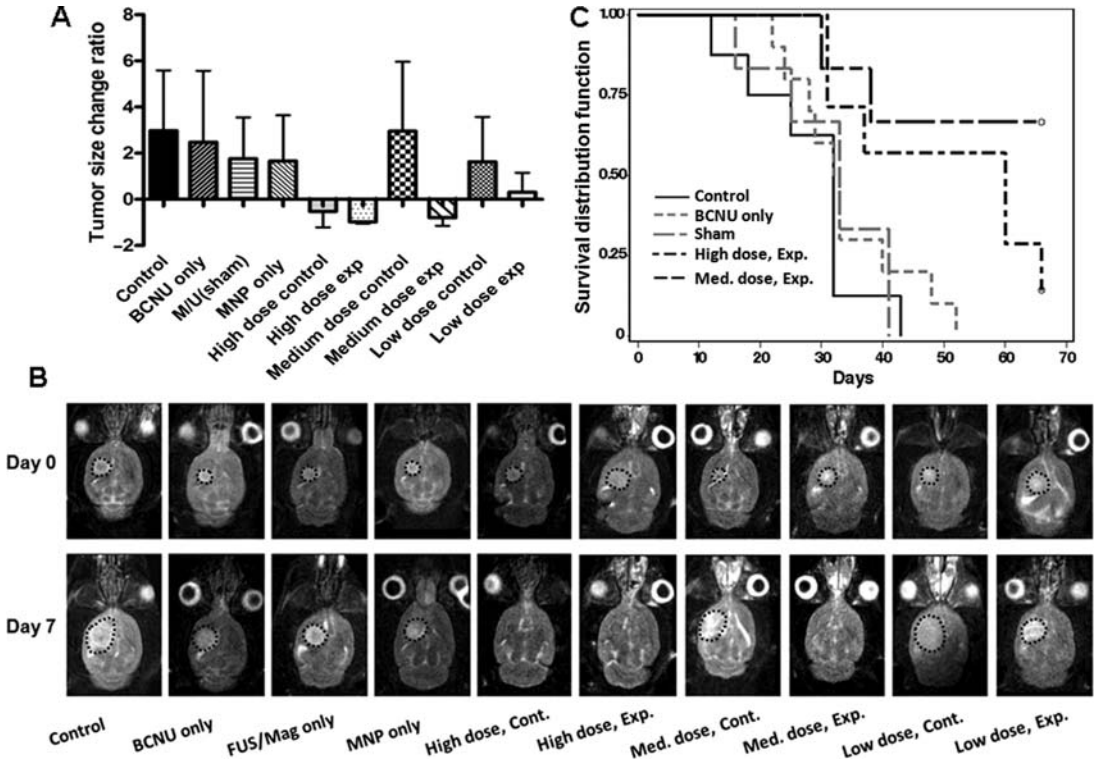

Fig. 5. (A) Ratios of average tumor volume changes in the first week after treatment. M/U, magnetic/ultrasound focusing treatment only; high dose, 5 mg immobilized BCNU/kg; medium dose, 1 mg immobilized BCNU/kg; low dose, 0.5 mg immobilized BCNU/kg; dose controls, without M/U treatment; dose exp, with M/U treatment. (B) Representative examples of longitudinal brain tumor monitoring using T2-weighted MRI of each group (Days 0 and 7 posttreatment). (C) Kaplan–Meier survival curves. Survival improvement at high and medium doses is statistically significant.

Table 2. Effect of in vivo treatment regimens on tumor volume

Group	Mean tumor volume (cm^3) ± *SD*		
	Day 0	Day 7	Mean $\Delta_{\text{tumor vol.}}$ ratio[a] ± *SD*
1	0.073 ± 0.038	0.235 ± 0.102	2.982 ± 2.606
2	0.048 ± 0.009	0.149 ± 0.100	2.482 ± 3.090
3	0.070 ± 0.035	0.164 ± 0.079	1.765 ± 1.790
4	0.080 ± 0.032	0.152 ± 0.091	1.149 ± 1.580
5	0.084 ± 0.039	0.059 ± 0.100	−0.519 ± 0.694[b]
6	0.156 ± 0.064	0.007 ± 0.016	−0.968 ± 0.078[b]
7	0.056 ± 0.020	0.190 ± 0.081	2.958 ± 3.002
8	0.173 ± 0.075	0.044 ± 0.071	−0.792 ± 0.351[b]
9	0.115 ± 0.045	0.252 ± 0.152	1.630 ± 1.941
10	0.136 ± 0.040	0.163 ± 0.115	0.309 ± 0.841[b]

[a] $\Delta_{\text{tumor vol.}}$ ratio = (Tumor $\text{vol}_{\text{day 7}}$ − Tumor $\text{vol}_{\text{day 0}}$)/Tumor $\text{vol}_{\text{day 0}}$. One-way ANOVA of $\Delta_{\text{tumor vol.}}$ ratio: $F = 4.062$, $P < 0.001$.
[b] Post hoc analysis: Differs significantly from Group 1 ($P < 0.05$).

magnetic effect, enhancing localization to specific tumor sites rather than delivering MNP-bound drugs more diffusely.

To determine the optimal enhancement conditions, different doses of BCNU–MNP were tested. Even without magnetic/ultrasound enhancement, treatment with an effective BCNU dose of 5 mg/kg (ie, Group 5) was more effective at shrinking tumors than was treatment with unbound BCNU at a dose of 13.5 mg/kg (Group 2). It is possible that MNPs induce the enhanced permeability and retention (EPR) effect.[37] Also, the increased BCNU concentration in tumor cells might not only result from diffusion, but also result from phagocytosis of drug-bound particles by the cells. In animals treated with an effective dose of 1 mg BCNU/kg, the EPR effect was apparently insufficient to produce an effective local therapeutic dose (Group 7), but treatment with the magnetic/ultrasound focusing system at this dose enhanced BCNU delivery sufficiently to induce tumor shrinkage (Group 8). Similarly, although at the lowest dose tested magnetic/ultrasound focusing did not shrink tumors, tumor growth was still slowed relative to animals treated with the same dose but not subjected to magnetic/ultrasound enhancement. Overall, it is estimated that the magnetic/ultrasound focusing system enhances drug delivery to tumors ~5-fold. This, however, is significantly less than the 26-fold enhancement of particle concentration seen in normal rat brains by ICP–OES. It is possible that some of the BCNU is hydrolyzed during intravenous circulation. Also, the tumor microenvironment is quite different from that of the normal brain; the altered vascular and

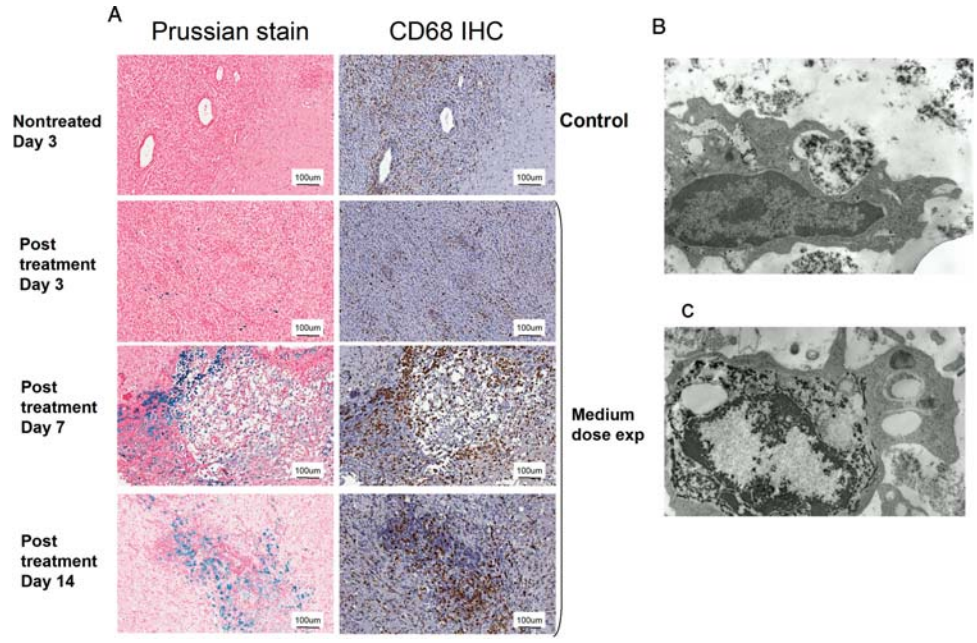

Fig. 6. Microscopic examination of control and treated brain tumor tissue. (A) Prussian blue staining of an untreated control tumor and a tumor at Days 3, 7, and 14 posttreatment. The adjacent serial sections were immmunostained with anti-CD68 and show evidence of macrophage infiltration after tumor disappearance. Transmission electron microscopy shows that iron particles also begin to accumulate in the cytoplasm of tumor cells (B) and apoptotic cells (C) as early as 1 day after treatment.

hemodynamic properties in tumors could reduce the efficacy of magnetic/ultrasound focusing.[6,38]

Effective treatment of induced tumors is expected to not only shrink the tumors, but also increase subject survivability. Interestingly, animals treated with the medium dose of BCNU–MNP survived longer than those treated with the higher dose. It is possible that the lower dose was less total toxic to other organs, but additional experiments are necessary to determine the precise cause of this phenomenon.

CD68-positive cells (possibly glioma-infiltrating macrophages) appear in tumors even before treatment. They can constitute up to 30% of the tumor mass and often are upregulated after various treatments.[39,40] The percentages of CD68-positive cells were similar in the control, sham, and particle-only groups, indicating that neither the MNPs nor magnet/ultrasound focusing induced tissue damage that might cause additional macrophage infiltration (data not shown). Immunohistochemistry on serial brain sections showed an increase in CD68-positive and other inflammatory cells during the later stages of tumor shrinkage. This could indicate clearing of both necrotic tumor debris and iron particles.

An additional significant advantage of this system is that the superparamagnetic properties of the iron oxide core of the BCNU–MNPs make it possible to track particle distribution in the brain by MRI. This allows the efficacy of the various treatment protocols on brain tumors to be assessed over time. Also, a certain level of quantification is attainable by measuring the intensity of the images.

In summary, our novel magnetic/ultrasound system enhances passive transport by transient disruption of the blood–brain barrier and magnetically stimulates active transport, increasing delivery of antineoplastic drugs to brain tumors. The method is noninvasive, reversible, and can be targeted with greater precision to a specific region of interest. Because the drugs are administered intravenously rather than intra-arterially or by direct cranial injection/implantation, the treatment is more practical in a clinical setting. It can be used before or after surgery, or even in cases where surgical intervention is not feasible. With this protocol, lower concentrations of drugs can be used to provide more efficient tumor suppression, concurrently reducing the likelihood of adverse systemic effects. Finally, the nature of the nanoparticles makes effective MRI monitoring of drug delivery and treatment possible. It should be noted that, although no seizures or other neurologic deficits were observed in successfully treated rats, the long-term effects of magnetic force, ultrasound, and iron deposited in the brain require further study. Nevertheless, this strategy provides a promising novel means for potentially useful chemotherapeutic drugs to cross the blood–brain barrier more efficiently and penetrate brain tumors more precisely.

Supplementary Data

Details of the preparation and characterization of nanoparticle-immobilized BCNU are available free of charge via the Internet at http://pubs.acs.org.

Acknowledgments

The authors thank Microscopy Core Laboratory of Chang-Gung Memorial Hospital and the pathology core of the Chang-Gung Molecular Medicine Research Center for technical support.

Conflict of interest statement. None declared.

Funding

This research was supported by National Health Research Institutes Research Grant NHRI-EX95-9507NI, Taiwan; Chang-Gung Memorial Hospital Researches Grant (CMRPG330983 CMRPD34022, CMRPD260041, CMRPD250013 and CMRPG350193), Taiwan; Department of Health, Taiwan, DOH98-TD-N-111-002; and National Science Council (NSC-95-2221-E-182-034-MY3).

References

1. Lin SH, Kleinberg LR. Carmustine wafers: localized delivery of chemotherapeutic agents in CNS malignancies. *Expert Rev Anticancer Ther*. 2008;8:343–359.
2. Pan E, Mitchell SB, Tsai JS. A retrospective study of the safety of BCNU wafers with concurrent temozolomide and radiotherapy and adjuvant temozolomide for newly diagnosed glioblastoma patients. *J Neurooncol*. 2008;88:353–357.
3. DeAngelis LM. Brain tumors. *N Engl J Med*. 2001;344:114–123.
4. Furnari FB, Fenton T, Bachoo RM, et al. Malignant astrocytic glioma: genetics, biology, and paths to treatment. *Genes Dev*. 2007;21:2683–2710.
5. Parney IF, Chang SM. Current chemotherapy for glioblastoma. *Cancer J*. 2003;9:149–156.
6. Begley DJ. Delivery of therapeutic agents to the central nervous system: the problems and the possibilities. *Pharmacol Ther*. 2004;104:29–45.
7. Neuwelt EA. Mechanisms of disease: the blood–brain barrier. *Neurosurgery*. 2004;54:131–140.
8. Karkan D, Pfeifer C, Vitalis TZ, et al. A unique carrier for delivery of therapeutic compounds beyond the blood–brain barrier. *PLoS ONE*. 2008;3:e2469.
9. Suidan GL, McDole JR, Chen Y, Pirko I, Johnson AJ. Induction of blood brain barrier tight junction protein alterations by CD8 T cells. *PLoS One*. 2008;3:e3037.
10. Monsky WL, Fukumura D, Gohongi T, et al. Augmentation of transvascular transport of macromolecules and nanoparticles in tumors using vascular endothelial growth factor. *Cancer Res*. 1999;59:4129–4135.
11. Doolittle ND, Miner ME, Hall WA, et al. Safety and efficacy of a multicenter study using intra-arterial chemotherapy in conjunction with osmotic opening of the blood–brain barrier for the treatment of patients with malignant brain tumors. *Cancer*. 2000;88:637–647.
12. Pardridge WM. Neurotrophins, neuroprotection and the blood–brain barrier. *Curr Opin Investig Drugs*. 2002;3:1753–1757.
13. Pardridge WM. Targeting neurotherapeutic agents through the blood–brain barrier. *Arch Neurol*. 2002;59:35–40.
14. Rautioa J, Chikhale PJ. Drug delivery systems for brain tumor therapy. *Curr Pharm Des*. 2004;10:1341–1353.
15. Alexiou C, Arnold W, Klein RJ, et al. Locoregional cancer treatment with magnetic drug targeting. *Cancer Res*. 2000;60:6641–6648.
16. Koo YE, Reddy GR, Bhojani M, et al. Brain cancer diagnosis and therapy with nanoplatforms. *Adv Drug Deliv Rev*. 2006;58:1556–1577.
17. Chertok B, David AE, Huang Y, Yang VC. Glioma selectivity of magnetically targeted nanoparticles: a role of abnormal tumor hydrodynamics. *J Control Release*. 2007;122:315–323.
18. Chertok B, Moffat BA, David AE, et al. Iron oxide nanoparticles as a drug delivery vehicle for MRI monitored magnetic targeting of brain tumors. *Biomaterials*. 2008;29:487–496.
19. Hynynen K, McDannold N, Vykhodtseva N, Jolesz FA. Noninvasive MR imaging-guided focal opening of the blood–brain barrier in rabbits. *Radiology*. 2001;220:640–646.
20. Mesiwala AH, Farrell L, Wenzel HJ, et al. High-intensity focused ultrasound selectively disrupts the blood–brain barrier in vivo. *Ultrasound Med Biol*. 2002;28:389–400.
21. Hynynen K, McDannold N, Vykhodtseva N, Jolesz FA. Non-invasive opening of BBB by focused ultrasound. *Acta Neurochir*. 2003;86(suppl.):555–558.
22. Hynynen K, McDannold N, Sheikov NA, Jolesz FA, Vykhodtseva N. Local and reversible blood–brain barrier disruption by noninvasive focused ultrasound at frequencies suitable for trans-skull sonications. *NeuroImage*. 2005;24:12–20.
23. McDannold N, Vykhodtseva N, Raymond S, Jolesz FA, Hynynen K. MRI-guided targeted blood–brain barrier disruption with focused ultrasound: histological findings in rabbits. *Ultrasound Med Biol*. 2005;31:1527–1537.
24. Liu H-L, Hua M-Y, Chen P-Y, et al. Blood–brain barrier disruption by focused ultrasound enhances delivery of chemotherapeutic drugs for glioblastoma treatment. *Radiology*. 2010;255:415–425.
25. Loo TL, Dion RL. Colorimetric method for the determination of 1,3-bis(2-chloroethyl)-1-nitrosourea. *J Pharm Sci*. 1965;54:809–810.
26. Kim GY, Tyler BM, Tupper MM, et al. Resorbable polymer microchips releasing BCNU inhibit tumor growth in the rat 9L flank model. *J Control Release*. 2007;123:172–178.
27. Magnitsky S, Watson DJ, Walton RM, et al. In vivo and ex vivo MRI detection of localized and disseminated neural stem cell grafts in the mouse brain. *NeuroImage*. 2005;26:744–754.
28. Arosarena O, Guerin C, Brem H, Laterra J. Endothelial differentiation in intracerebral and subcutaneous experimental gliomas. *Brain Res*. 1994;640:98–104.
29. Blasberg RG, Molnar P, Horowitz M, Kornblith P, Pleasants R, Fenstermacher J. Regional blood flow in RT-9 brain tumors. *J Neurosurg*. 1983;58:863–873.
30. Pathak AP, Schmainda KM, Ward BD, Linderman JR, Rebro KJ, Greene AS. MR-derived cerebral blood volume maps: issues regarding histological validation and assessment of tumor angiogenesis. *Magn Reson Med*. 2001;46:735–747.
31. Pulfer SK, Gallo JM. Enhanced brain tumor selectivity of cationic magnetic polysaccharide microspheres. *J Drug Target*. 1998;6:215–227.
32. Lesniak MS, Brem H. Targeted therapy for brain tumours. *Nat Rev Drug Discov*. 2004;3:499–508.
33. Groothuis DR, Fischer JM, Lapin G, Vick NA, Bigner DD. Permeability of different experimental brain tumor models to horseradish peroxidase. *J Neuropathol Exp Neurol*. 1982;41:164–185.

34. Neuwelt EA, Barnett PA, Bigner DD, Frenkel EP. Effects of adrenal cortical steroids and osmotic blood–brain barrier opening on methotrexate delivery to gliomas in the rodent: the factor of the blood–brain barrier. *Proc Natl Acad Sci USA*. 1982;79:4420–4423.
35. Neuwelt EA, Frenkel EP, D'Agostino AN. Growth of human lung tumor in the brain of the nude rat as a model to evaluate antitumor agent delivery across the blood-brain barrier. *Cancer Res*. 1985;45:2827–2833.
36. Neuwelt EA, Howieson J, Frenkel EP, et al. Therapeutic efficacy of multiagent chemotherapy with drug delivery enhancement by blood-brain barrier modification in glioblastoma. *Neurosurgery*. 1986;19:573–582.
37. Maeda H, Wu J, Sawa T, Matsumura Y, Hori K. Tumor vascular permeability and the EPR effect in macromolecular therapeutics: a review. *J Control Release*. 2000;65:271–284.
38. Huang B-R, Chen P-Y, Huang C-Y, et al. Bioavailability of magnetic nanoparticles to the brain. *J Magn Magn Mater*. 2009;321:1604–1609.
39. Fulci G, Dmitrieva N, Gianni D, et al. Depletion of peripheral macrophages and brain microglia increases brain tumor titers of oncolytic viruses. *Cancer Res*. 2007;67:9398–9406.
40. Okada H, Kohanbash G, Zhu X, et al. Immunotherapeutic approaches for glioma. *Crit Rev Immunol*. 2009;29:1–42.